Improved Properties of Highly Oriented Graphene/Polymer Nanocomposites

Peng-Gang Ren,[1] Ding-Xiang Yan,[2] Tao Chen,[3] Bao-Qing Zeng,[3] Zhong-Ming Li[2]

[1]*Institute of Printing and Packaging Engineering, Xi'an University of Technology, Xi'an, Shaanxi 710048, People's Republic of China*
[2]*State Key Laboratory of Polymer Materials Engineering, College of Polymer Science and Engineering, Sichuan University, Chengdu, Sichuan 610065, People's Republic of China*
[3]*Vacuum Electronics National Laboratory, School of Physical Electronics, University of Electronic Science and Technology of China, Chengdu 610054, People's Republic of China*

Received 20 September 2010; accepted 30 November 2010
DOI 10.1002/app.33856
Published online 6 April 2011 in Wiley Online Library (wileyonlinelibrary.com).

ABSTRACT: A kind of molecular-level dispersed and highly oriented graphene monolayer nanocomposite film was successfully obtained by *in situ* reduction of phenyl isocyanate functionalized graphite oxide (RPIGO) in *N,N*-dimethylformamide in the presence of polystyrene (PS). Atomic force microscopy and transmission electron microscopy results show that the RPIGO monolayers were not only homogeneously intercalated into the PS matrix but also arranged parallel to the surface of the nanocomposite films. Because of the efficient interaction between the graphene monolayers and PS matrix, the mechanical properties of the graphene-based nanocomposite films improved significantly. Compared with the pure PS film, a 28.4% increase in the Young's modulus and a 27.8% improvement in the tensile strength of the RPIGO–PS nanocomposites films were obtained with the addition of only 0.5 wt % graphite oxide. The glass-transition temperature and onset degradation temperature of PS also increased from 96.6 and 427°C to 103.2 and 439°C, respectively. The improvement of the properties was mainly due to the large lateral thickness ratio and the high orientation of graphene monolayers. © 2011 Wiley Periodicals, Inc. J Appl Polym Sci 121: 3167–3174, 2011

Key words: films; mechanical properties; monolayers; nanocomposites; TEM

INTRODUCTION

Graphene exhibits remarkable properties, such as a high Young's modulus (~ 1100 GPa), fracture strength (125 GPa), thermal conductivity (~ 5000 W m^{-1} K^{-1}), mobility of charge carriers (200,000 cm^2 V^{-1} s^{-1}), specific surface area (calculated value = 2630 m^2/g),[1,2] higher lateral thickness ratio, and a lower cost compared to that of carbon naontubes. Therefore, graphene is considered a promising nanoscale filler for next-generation nanocomposite materials, offering nanocomposites with higher performances.[3–8] The preparation of such nanocomposites requires that graphene sheets be homogeneously distributed in the matrix. Unfortunately, graphene sheets are hydrophobic and are easily agglomerated in many organic solvents. In graphite oxide (GO), many strongly hydrophilic groups, including hydroxyls, epoxides, diols, ketones, and carboxyls, significantly alter the van der Waals interactions between the layers of graphene. Hence, GO can be easily exfoliated in water or polar aprotic solvents [e.g., *N,N*-dimethylformamide (DMF)] at the monolayer level, particularly, with the help of isocyanate.[9–11] Therefore, although graphene has been successfully obtained by chemical vapor deposition and epitaxial growth,[12,13] micromechanical exfoliation of graphite,[14] and so on, the production of graphene from colloidal suspensions composed of GO is still considered to be the most effective way to produce graphene monolayers on a large scale.[1–3]

Like carbon nanotubes, the practical challenge in the fabrication of GO–polymer nanocomposites is the homogeneous dispersion of GO in the host polymer matrix. DMF is a common solvent for both GO and polystyrene (PS) and provides the conditions for the homogeneous dispersion of GO. Therefore, graphene–PS nanocomposites are very attractive to the scientific community.[5–7,15–18] Unfortunately, the functionalized epoxy or hydroxyl groups transform carbon atoms from a planar sp^2-hybridized to a distorted sp^3-hybridized; this results in an electric insulator of GO. Conductive graphene–PS nanocomposites can only be obtained by the reduction of the

Correspondence to: P.-G. Ren (rengpg@126.com) or Z.-M. Li (zmli@scu.edu.cn).

Contract grant sponsor: National Outstanding Youth Foundation of China; contract grant number: 50925311.
Contract grant sponsor: National Foundation of China; contract grant number: 51073128.
Contract grant sponsor: Xi'an University of Technology; contract grant number: 104-210906.

GO–PS solution. The excellent electrical conductivity of graphene–PS nanocomposites (with a percolation threshold of only 0.1 vol % and an electrical conductivity as high as 0.1 S/m at 1 vol %[5]) allows one to consider them as a most promising functional conductive material. For practical applications, both the mechanical and thermal properties are important. Maximal mechanical enhancement can be achieved only when the graphene monolayers are homogeneously distributed and highly oriented in the polymer matrix. The available literature overwhelmingly reports the dispersion efficiency of GO in solvents and the electrical conductivity of reduced graphite oxide (RGO)–PS nanocomposites, but few studies have been focused on the major properties of graphene–PS nanocomposites, such as the mechanical properties and thermal stability.

In this study, GO was prepared by a modified Hummers method and characterized by atomic force microscopy (AFM) and transmission electron microscopy (TEM). Then, molecular-level and highly oriented graphene–PS nanocomposites were obtained with the modified well-established fabrication method.[5] The mechanical and thermals properties of the nanocomposites were studied by tensile testing, dynamic mechanical analysis, and thermogravimetric analysis (TGA). The results show that the mechanical and thermal properties of PS were efficiently enhanced with the addition of graphene.

EXPERIMENTAL

Materials

Expanded graphite (EP; expansion rate = 200 mL/g) and PS were obtained from Qingdao Haida Graphite Co., Ltd., (Qingdao, China) and Fushun Petroleum and Chemical Industry (Fushun, China), respectively. Phenyl isocyanate (PI) was obtained from Shanghai DEMO Chemical Co., Ltd. (Shanghai, China).

Sample preparation

Preparation of the GO platelets

GO was prepared by a modified Hummers method from EP. EP (10 g) and concentrated H_2SO_4 (230 mL) were placed in a flask. $KMnO_4$ (30 g) was added gradually with stirring in an ice-water bath. Then, the mixture was stirred at 35°C for 2 h, and distilled water (460 mL) was added. After 1 h, the reaction was terminated by the addition of a large amount of distilled water (1.4 L) and a 30% H_2O_2 solution (25 mL), after which the color of the suspension changed to bright yellow. The suspension was washed with a 1 : 10 HCl solution (2.5 L) by filter paper and funnel. The paste collected from the filter paper was dried at 60°C until the agglomerate appeared. The agglomerate was dispersed into distilled water in the static state for 2–3 h and stirred slightly by a glass bar. The suspension was washed with distilled water repeatedly with filter paper and a funnel until the pH was close to 7. The paste collected from the filter paper was dispersed into water by ultrasonication. The obtained brown dispersion was then subjected to 30 min of centrifugation at 4000 rpm to remove any unexfoliated GO with a centrifuge with a rotor radius of 14 cm. Finally, the GO platelets were obtained by dehydration at 60°C in air.

Fabrication of the nanocomposite films

Dried GO (200 mg) was suspended in anhydrous DMF (100 mL) and treated with PI (4 mmol) for 48 h. Then, a PS/DMF solution (0.1 g/mL) was added to the mixture. Reduction was carried out by hydrazine (hydrazine/GO weight ratio = 1) at 90°C for 5 h. Stirring and intermittent ultrasonic dispersion were continued throughout the whole preparation process. Upon completion, the mixture was added dropwise into a large volume of stirred distilled water (10 : 1 with respect to the volume of DMF used). The coagulation of the RGO–PS nanocomposites was obtained. This coagulation powder was isolated via filtration, washed with distilled water three times, dried at 130°C for 24 h to remove residual solvent, and then pressed in a hot press under 10 MPa at a temperature of 160°C for 5 min.

Characterization

X-ray photoelectron spectroscopy (XPS)

XPS analysis was performed with an XSAM800 (Kratos Co., Manchester, UK) with Al Kα radiation (The energy of Mono Al X-ray source $h\nu = 1486.6$ eV); XPSpeak41 software (Hong Kong, China) was used to perform curve fitting and to calculate the atomic ratios.

AFM

AFM images were taken on a Nanoscope Multimode & Explore atomic force microscope (Veeco Instruments, Santa Barbara, California, USA). Imaging was done in tapping mode with a V-shaped Ultralever probe B (Veeco Instruments, Santa Barbara, California USA). All images were collected under ambient conditions at 50% relative humidity and 18°C with a scanning raster rate of 2 Hz. We prepared samples for the AFM images by dropping the dispersion of GO in DMF on a freshly cleaved Si surface (Ted Pella, Inc., Redding, California USA) and allowing them to dry in air.

TEM

TEM was performed with a Philips T20ST electron microscope (Eindhoven, Netherlands) at an acceleration

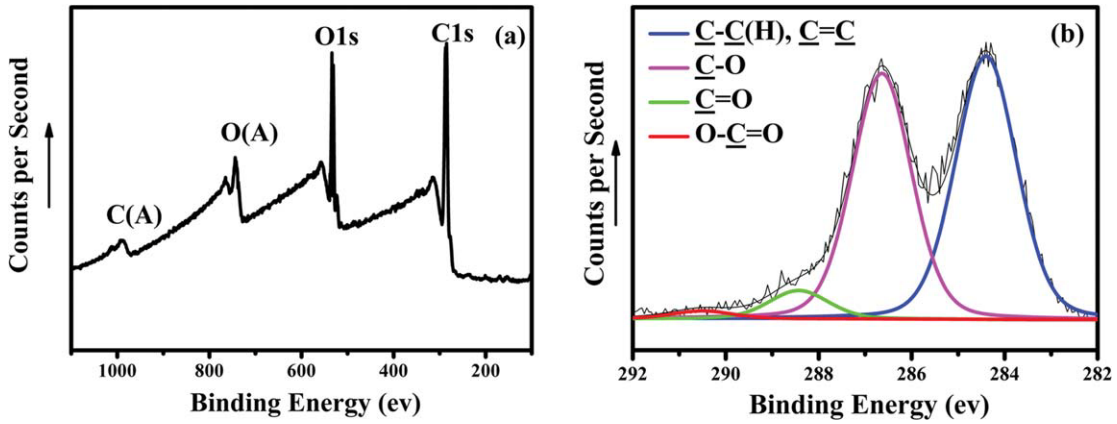

Figure 1 (a) XPS survey spectrum and (b) deconvolution of the C1s peak for GO. [Color figure can be viewed in the online issue, which is available at wileyonlinelibrary.com.]

voltage of 200 kV. The solution was dropped onto carbon-coated copper grids (mesh size = 300) and dried under ambient conditions.

TGA

TGA was carried out with a Seiko EXSTAR6000 thermogravimetric analyzer (Seiko Instruments Inc., Chiba, Japan). The heating rate was 5°C/min. Each time, a sample of approximately 5 mg was measured in an aluminum crucible under N_2 from room temperature to 600°C. The samples were run in duplicate, and the curve was drawn with the average value from two TGA data.

Dynamic mechanical analysis (DMA)

DMA was carried out with a Q800 DMA instrument (TA Instruments, Headquartered, New Castle, USA) at heating rate of 3°C/min. The sample size was 35 × 4 × 0.2 mm^3. The testing range was from 5 to 150°C. The storage modulus and tangent of the loss angle were obtained, and the glass-transition temperature (T_g) was taken from the peak temperature (T_p) of the tan δ curve.

Mechanical properties testing

The mechanical properties of the nanocomposite films were measured with a Testometric Materials testing machine (Testometric Company Ltd. Rochdale, Lancashire. UK) according to ASTM D 638. The crosshead speed was 20 mm/min. All samples were cut into strips of 50 × 15 × 0.2 mm^3 with a razor blade.

RESULTS AND DISCUSSION

Dispersion of the phenyl isocyanate functionalized graphite oxide (PIGO) monolayers into the PS matrix

The XPS survey spectrum and deconvolution of the C1s peak for GO are shown in Figure 1. The C/O atomic ratio of GO obtained from XPS was 3.0; this indicated that some oxygen-containing groups were introduced into the graphite during oxidation, which disrupted the sp^2-bonded carbon network of the graphite. The results were consistent with that of the Raman spectrum. Two peaks at a binding energy of about 284.4 and 286.7 eV for GO, as shown in Figure 1(b), were assigned to graphitic C=C (C—C) and oxygen-containing functional groups. The deconvolution of the C1s peak of GO gave four peaks located at binding energies of 284.4, 286.7, 288.4, and 290.5 eV; these were assigned to the *C*—H (*C*—C, *C*=*C*), C—OH (or epoxide), *C*=O (carbonyl C), and O=*C*—OH (carboxylate C) functional groups, respectively. The strong intensity peak at 286.7 eV indicated that most oxygen-containing functional groups in GO were hydroxyl (C—OH) or epoxide (*C*—O—*C*) groups.

A typical AFM image of the GO monolayers from the DMF solution is shown in Figure 2(a). Clearly, the GO platelets were satisfactorily exfoliated in DMF and existed in the form of individual monolayers. Despite the different sizes, the large GO monolayers could reach 500 nm in their lateral direction. Most of the GO monolayers had a height of about 1.1 nm [Fig. 2(b)]. Theoretically, the height of graphene monolayers was close to 0.34 nm, but the presence of isolated epoxide and hydroxyl groups made the GO monolayers bump and wrinkle and increased the GO height to around 1 nm.[19]

Both suspensions of GO and PIGO–PS (0.5 wt %) in DMF remained a stable state, even after 30 days, because of the strong interaction between the oxygen-containing functional groups of GO and DMF (as shown in Fig. 3). The intercalation of DMF molecules into GO monolayers made the gap between the GO monolayers exceed the maximum size of agglomeration. Unfortunately, when GO was reduced by hydrazine, the dramatically declined interaction between the GO monolayer and DMF immediately induced the agglomeration of the

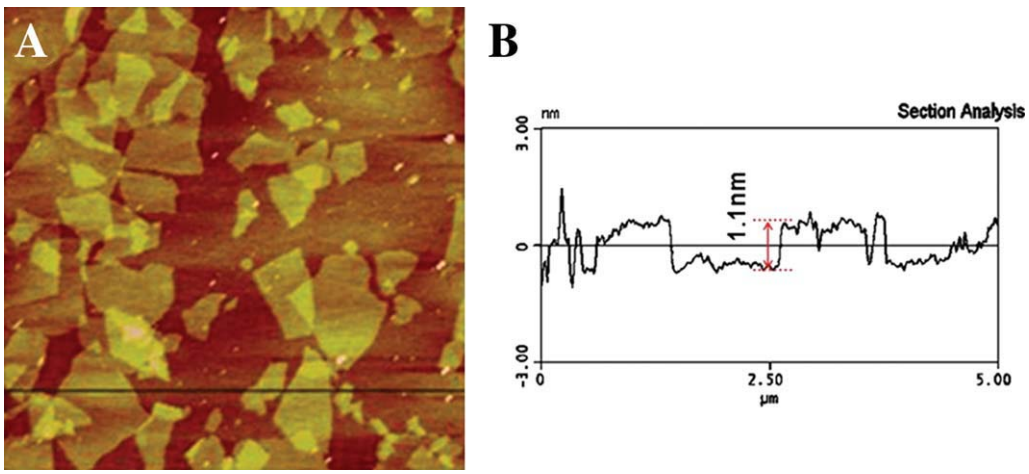

Figure 2 Typical AFM tapping-mode image of the GO monolayers from DMF dispersion. [Color figure can be viewed in the online issue, which is available at wileyonlinelibrary.com.]

GO/DMF colloidal suspension [Fig. 3(a)]. Compared with the GO colloidal suspension, the PIGO–PS colloidal suspension reduced by hydrazine would not agglomerate but formed two layers after 15 days, which was easily commixed by slight stirring [Fig. 3(b)]. All of the RGO monolayers located in the upper layer showed that the density of the RGO-containing layer decreased greatly. It is well known that the density of graphene (ca. 2.20 g/cm^3) is much higher than that of DMF (0.94 g/cm^3) and PS (1.05 g/cm^3).[5] Therefore, we concluded that the RGO monolayers were not only intercalated by PS molecules but also contained much interspace, which was occupied by the DMF molecules.

To obtain a molecular-level dispersed graphene nanocomposite, the presence of the polymer in the suspension during the reduction step is necessary. It means that the intercalation of polymer molecules into the GO monolayers must precede the reduction step (as shown in Fig. 4). PI has a strong affinity toward PS molecules via the interaction of the benzene rings between PS and PI. A number of PS molecules easily intercalate into the GO monolayers, which are covered by PI molecules on both sides. Although the interaction between RGO monolayers and PS molecules decreased after the reduction by hydrazine, the RGO monolayers were still dispersed on the molecular level in the PS matrix. The intercalated PS molecules could prevent the RGO monolayers from agglomerating. Thus, the molecular-level nanocomposites were obtained (method 1). When the reduction step precedes the intercalation of PS molecules

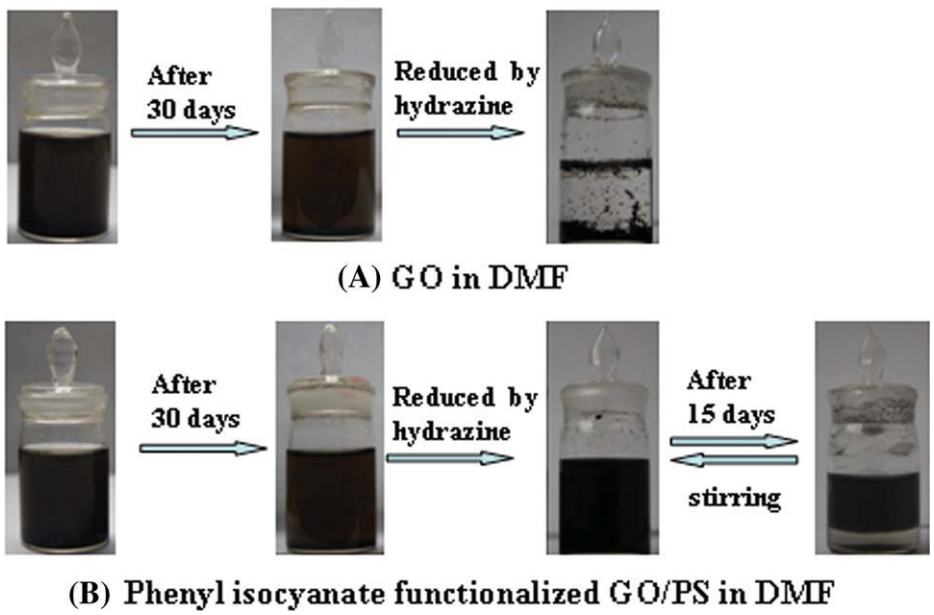

Figure 3 Dispersions of the (a) GO and (b) PIGO/PS (0.5 wt %) colloidal suspensions in DMF. [Color figure can be viewed in the online issue, which is available at wileyonlinelibrary.com.]

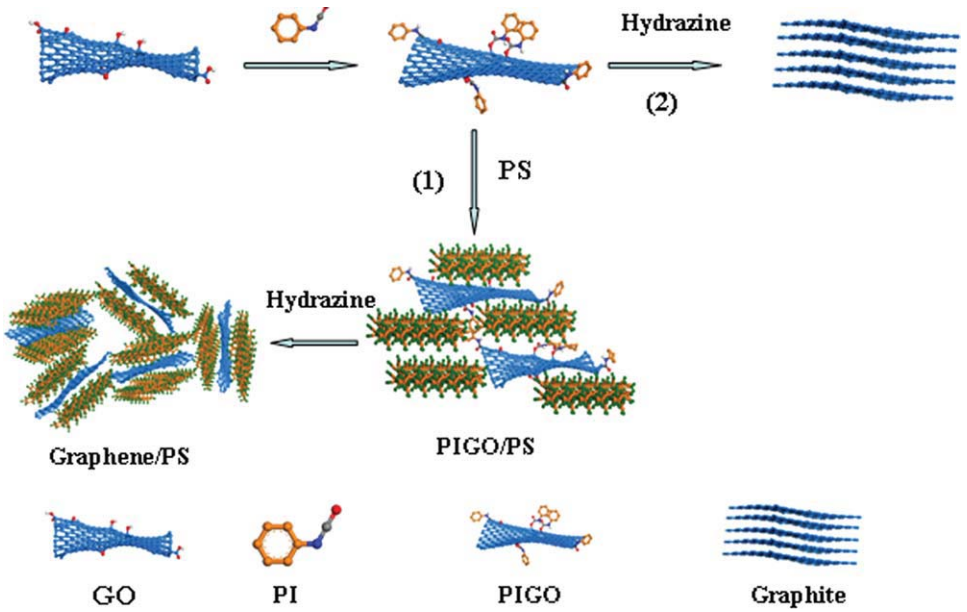

Figure 4 Structural transformations during the process of preparing the RPIGO–PS nanocomposites. [Color figure can be viewed in the online issue, which is available at wileyonlinelibrary.com.]

into the GO monolayers, the RGO monolayers agglomerated immediately. The PS molecules were not able to be intercalated into the RGO layers because of the stronger van der Waals interactions between the layers of graphene and could not form the molecular-level nanocomposites (method 2).

To verify the homogeneous dispersion of RGO monolayers in the PS matrix, TEM measurement was used for the phenyl isocyanate functionalized graphite oxide (RPIGO)–PS composite, as shown in Figure 5. The regular geometrical contour and uniform luminance of RGO with lateral dimensions around 500 nm was clearly observed in the TEM image; this, indeed, confirmed a fully exfoliated and successful dispersion of RGO monolayers in the PS matrix. Most of the RGO monolayers arranged along the film direction confirmed that the RGO monolayers were highly oriented in the nanocomposites.

The RGO monolayers were wrinkled rather than flat; this was confirmed by the RGO monolayer at the bottom of Figure 5 and by the shape and gray luminance of the edge of the other RGO monolayers. The wrinkled RGO monolayers might have increased the interspace between the PS molecules and RGO monolayers and, thus, reduced the density of the RPIGO–PS layer.

Mechanical and thermal properties of the RPFGO–PS nanocomposite films

We expected that the mechanical and thermal properties of these graphene-based nanocomposites would be significantly enhanced by the molecular-level dispersion and the high orientation of the graphene monolayers in the PS matrix. Figure 6 shows the DMA curves of PS and its graphene-based nanocomposite films, from which one can see that the storage modulus and T_g of the RPIGO–PS nanocomposites both improved significantly with increasing GO content. With only 0.1 wt % GO, the storage modulus of the nanocomposite films was improved by 26.5%, from 2190 to 2770 MPa. When the GO loading increased to 0.5 wt %, the storage modulus of the nanocomposite films increased by 47.9%, and T_g increased by about 6.6°C from 96.6 to 103.2°C.

In addition, the storage modulus of the RPIGO–PS nanocomposite films decreased obviously under low temperatures (5–70°C) compared to that of pure PS.

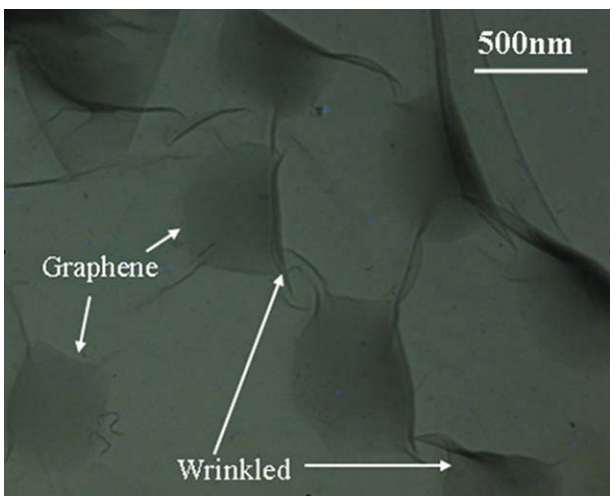

Figure 5 TEM micrographs of the RPIGO–PS nanocomposites (0.5 wt %). [Color figure can be viewed in the online issue, which is available at wileyonlinelibrary.com.]

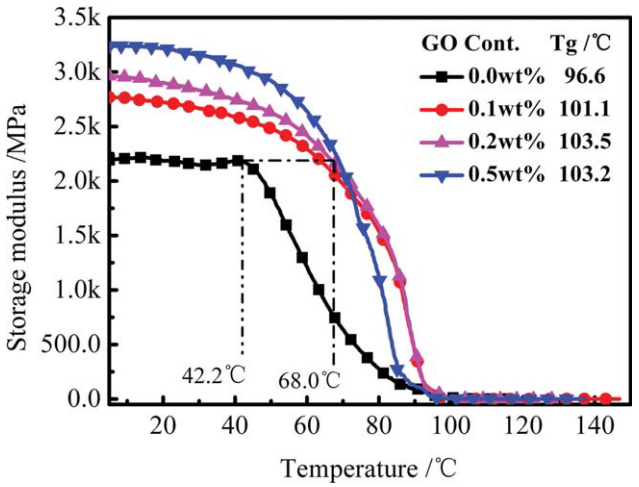

Figure 6 MDA curves of the PS and RPIGO–PS nanocomposites with tensile mode. [Color figure can be viewed in the online issue, which is available at wileyonlinelibrary.com.]

At the same time, the storage modulus of the graphene/PS decreased obviously when the GO content increased. This may have been due to the high thermal conductivity of the graphene monolayers. Compared to that of the graphene-based nanocomposite films, the internal temperature of the PS film was lower at the testing process because of the different thermal conductivity between the graphene monolayers and PS matrix; this resulted in the storage modulus of the PS film decreasing slowly over that of the graphene-based composites at the initial testing stage. Although the storage modulus of the PS film almost remained constant below 45°C, the residual value was only half of its original value at 60°C. However, the storage modulus of the RPIGO–PS nanocomposite film (0.1 wt %) still remained at 2200 MPa at 68.0°C, which was identical to the original value of PS. This indicated that in the requirement of high mechanical properties, the service temperature of PS could be increased by about 25.8°C with only 0.1 wt % GO.

The typical stress–strain curves of the PS and RPIGO–PS nanocomposite films are shown in Figure 7(a). The tensile strength and modulus of the RPIGO–PS nanocomposite films were both enhanced with increasing graphene content. With the addition of only 0.5 wt % GO, increments of 27.8 and 28.4% were obtained for the tensile strength and modulus, respectively, of the RPIGO–PS nanocomposite films; the tensile strength increased from 19.4 to 24.8 MPa, and the tensile modulus increased from 1.76 to 2.26 GPa. The elongation at break decreased by 9.77% from 1.33 to 1.20.

Figure 7(b) displays the improvement ratios of the strength and modulus of the experimental and theoretical values. The tensile modulus values of the RPIGO–PS nanocomposite films ($E_{\|}$) were simulated with the Halpin–Tsai model, which is widely used for predicting the modulus of unidirectionally distributed filler-reinforced nanocomposites.[20,21] $E_{\|}$ is given as follows:

$$E_{\|} = E_m\left[\frac{1+\eta_L\xi V_c}{1-\eta_L V_c}\right] \quad (1)$$

$$\eta_L = \frac{(E_g/E_m)-1}{(E_g/E_m)+\xi} \quad (2)$$

$$\xi = 2l_g/3t_g \quad (3)$$

where $E_{\|}$ represents the Young's modulus of nanocomposites with filler aligned parallel to the surface of the film sample; E_g and E_m are the Young's modulus of the filler and the polymer matrix, respectively; η_L is a factor depends on the reinforcement and matrix; ξ is a measure of reinforcement geometry which depends on loading conditions; l_g and t_g

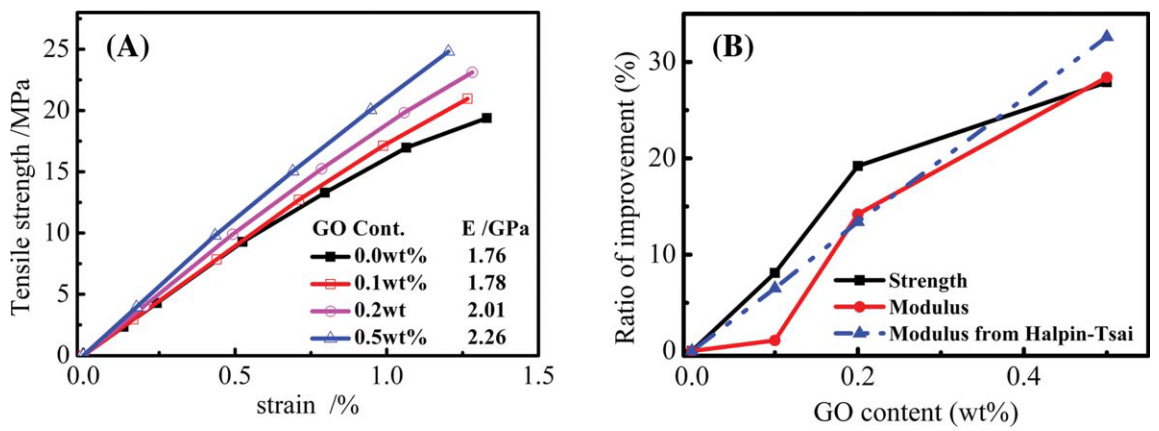

Figure 7 Mechanical properties of the PS and its nanocomposites. (E: Tensile modulus of PS and its nanocomposites). [Color figure can be viewed in the online issue, which is available at wileyonlinelibrary.com.]

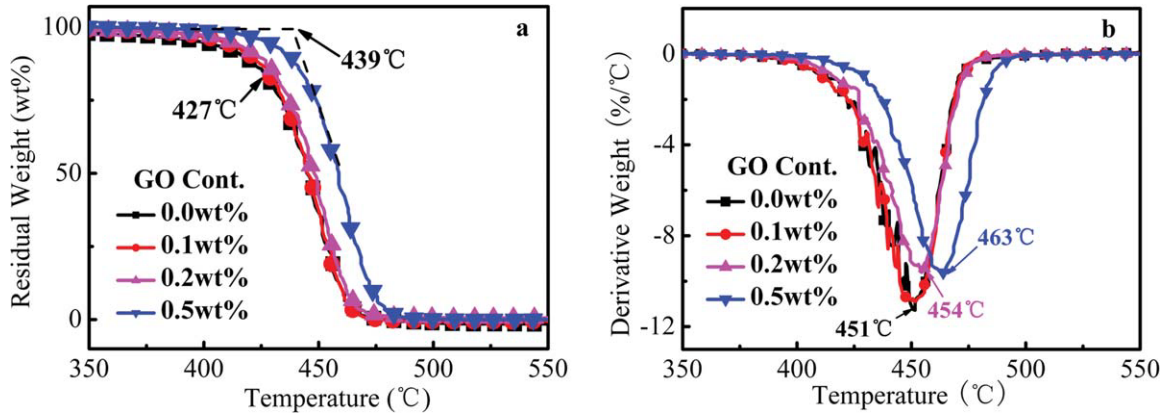

Figure 8 Thermal properties of the PS and RPIGO–PS nanocomposites: (a) TGA curves of the RPIGO–PS nanocomposites under N_2. (b) DTG curves of the RPIGO–PS nanocomposites under N_2. [Color figure can be viewed in the online issue, which is available at wileyonlinelibrary.com.]

refer to the length and thickness, respectively, of the filler; and V_c is the volume fraction of filler in the nanocomposites. In our study, the Young's modulus of the graphene was selected as 250 GPa, which was measured previously.[3] The Young's modulus of pure PS was 1.76 GPa from the experimental data. To convert the loading of graphene in weight percentage to volume percentage, the density of the PS matrix was assumed to be 1.5 g/cm^3, and the density of graphene was 2.2 g/cm^3. l_g and t_g of the graphene sheet were about 500 and 0.34 nm, respectively, as determined by AFM analysis and a literature report.[19] Thus, the Young's modulus of the nanocomposites was calculated.

$E_{\|}$ was in line with the results from the Halpin–Tsai model simulation under the hypothesis that the graphene monolayer was aligned parallel to the surface of the nanocomposite films. This good agreement indicated that the graphene monolayers not only were homogeneously distributed with high orientation along the film direction but also had strong interfacial adhesion with the PS molecules.

The TGA and differential thermogravimetry (DTG) curves of PS and its nanocomposite films under nitrogen gas conditions are shown in Figure 8 (to survey clearly, only segmental curves are displayed). The onset degradation temperature of the nanocomposite films shifted toward a higher temperature compared to that of pure PS. Although the improvement of the onset degradation temperature of the nanocomposite films was difficult to detect at a low content of GO, an abrupt change of onset degradation temperature occurred at contents of GO greater than 0.2 wt %. With 0.5 wt % GO loading, the onset degradation temperature increased by 12°C from 427°C (PS) to 439°C [Fig. 8(a)]. The T_p's of the DTG curves are shown in Figure 8(b). The T_p values of the nanocomposite films with 0.1, 0.2, and 0.5 wt % GO also increased by about 0, 3, and 12°C from 451 to 451, 454, and 463°C, respectively, as compared with the pure PS film.

Enhancement mechanism

The mechanism behind the enhancement of the mechanical and thermal properties of nanocomposites was attributed to the strong interaction between the PS molecules and PIGO and the excellent mechanical properties, large lateral thickness ratio, and alignment of the graphene monolayers. Graphene is a flat monolayer of carbon atoms tightly packed into a honeycomb lattice, which made the graphene monolayers enwrapped with polymer liable to arrange along the parallel direction to the nanocomposites film during the hot-pressing process. Thus, layer-by-layer graphene-based nanocomposites were obtained (as shown in Fig. 9).

Moreover, PI not only reacted with the carboxyl and hydroxyl groups of GO but also had a strong affinity to PS molecules via the interaction of benzene rings between PS and PI. Thus, the modulus and strength of the nanocomposites were improved by the highly oriented graphene monolayers and the strong interfacial interaction between PS and PIGO. As the graphene monolayers were dispersed on the molecular level in the PS matrix, although the

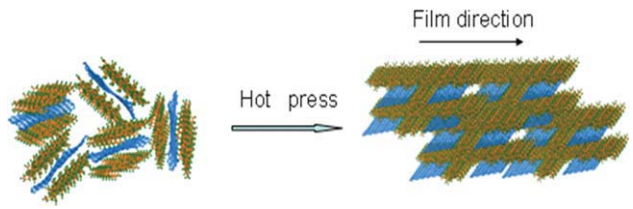

Figure 9 Arrangement of the graphene monolayers along film direction during the hot-pressing procedure. [Color figure can be viewed in the online issue, which is available at wileyonlinelibrary.com.]

content of graphene was very low, a large number of graphene monolayers were still incorporated into the PS matrix. Because of the large lateral thickness ratio and high modulus, the graphene monolayers the PS matrix were considered to be rigid graft groups, which restricted the movement of PS chain segments and molecules and led to the prominent improvement of T_g at low loadings of GO. The improvement of the thermal stability of the graphene–PS nanocomposites may have originated from the excellent barrier properties and high orientation of graphene. For gas permeability through a polymer filled with a high aspect ratio, impermeable flakes can be decreased substantially via a reduced cross section for gas diffusion and a tortuous path mechanism.[22] A barrier model for gas permeability of membranes filled with aligned monodispersed impermeable disks was made by Lape et al.,[23] who predicted that polymer films with aligned impermeable flakes could have permeabilities 100 times smaller than that of the pure polymer films. Because of the tightly packed honeycomb lattice and arrangement along the film of graphene, it was speculated that the gas permeability of the PS membrane would obviously decrease with the addition of graphene. This result has been proved in some studies.[22,24] So the gases produced by thermal decomposition were difficult to volatilize from the RPIGO–PS nanocomposite films; this led to the improvement of thermal stability of the graphene–PS nanocomposites. At low loadings of GO (<0.2 wt %), the descent of gas permeability was insufficient to prevent the volatilization of decomposition gas, so the onset degradation temperature and T_p of the nanocomposites hardly increased. When the contents of GO exceeded a critical value (0.5 wt %), the enormously reduced cross section and increased tortuous path for gas diffusion significantly improved the onset temperature and T_p of the nanocomposites[as see Fig. 8(a,b)].

CONCLUSIONS

With the aid of ultrasonic dispersion, the GO prepared by a modified Hummers method from EP was completely exfoliated down to the monolayers in DMF. The AFM image showed that the thickness of the GO monolayers was about 1.1 nm, and the lateral extent was about 500 nm. The TEM results indicate that molecular-level nanocomposites could be obtained by the intercalation of PS molecules into PIGO monolayers before the reduction step. The mechanical properties of the molecular-level RPIGO–PS nanocomposites increased with increasing concentration of GO. With only 0.5 wt % GO loading, the tensile modulus, tensile strength of PS increased from 19.4 MPa and 1.76 GPa to 24.8 MPa and 2.26 GPa and increased by 28.4 and 27.8%, respectively. T_g and the onset degradation temperature of PS also increased from 96.6 and 427 to 103.2 and 439°C, respectively. The enhancement of the mechanical and thermal properties of the nanocomposites with such low contents was attributed to the excellent modulus, large lateral thickness ratio, and high orientation of the graphene sheets, which not only restricted the movement of PS chain segments and molecules but also blocked the permeation of gases produced by thermal decomposition.

References

1. Park, S. J.; Ruoff, R. S. Nat Nanotechnol 2009, 4, 217.
2. Dikin, D. A.; Stankovich, S.; Zimney, E. J.; Piner, R. D.; Dommett, G. H. B.; Evmenenko, G.; Nguyen, S. T.; Ruoff, R. S. Nature 2007, 448, 457.
3. Rao, C. N. R.; Sood, A. K.; Subrahmanyam, K. S.; Govindaraj, A. Angew Chem Int Ed 2009, 48, 7752.
4. Geim, A. K.; Novoselov, K. S. Nat Mater 2007, 6, 183.
5. Stankovich, S.; Dikin, D. A.; Dommett, G. H. B.; Kohlhaas, K. M.; Zimney, E. J.; Stach, E. A.; Piner, R. D.; Nguyen, S. T.; Ruoff, R. S. Nature 2006, 442, 282.
6. Ramanathan, T.; Abdala, A. A.; Stankovich, S.; Dikin, D. A.; Herrera-Alonso, M.; Piner, R. D.; Adamson, D. H.; Schniepp, H. C.; Chen, X.; Ruoff, R. S.; Nguyen, S. T.; Aksay, I. A.; Prud'Homme, R. K.; Brinson, L. C. Nat Nanotechnol 2008, 3, 327.
7. Watcharotone, S.; Dikin, D. A.; Stankovich, S.; Piner, R.; Jung, I.; Dommett, G. H. B.; Evmenenko, G.; Wu, S. E.; Chen, S. F.; Liu, C. P.; Nguyen, S. T.; Ruoff, R. S. Nano Lett 2007, 7, 1888.
8. Wei, T.; Luo, G. L.; Fan, Z. J.; Zheng, C.; Yan, J.; Yao, C. Z.; Li, W. F.; Zhang, C. Carbon 2009, 47, 2296.
9. Park, S. J.; An, J. H.; Jung, I.; Piner, R. D.; An, S. J.; Li, X. S.; Velamakanni, A.; Rouff, R. S. Nano Lett 2009, 9, 1593.
10. Paredes, J. I.; Villar-Rodil, S.; Martinez-Alonso, A.; Tascon, J. M. D. Langmuir 2008, 24, 10560.
11. Li, D.; Muller, M. B.; Gilje, S.; Kaner, R. B.; Wallace, G. G. Nat Nanotechnol 2008, 3, 101.
12. Land, T. A.; Michely, T.; Behm, R. J.; Hemminger, J. C.; Comsa, G. Surf Sci 1992, 264, 261.
13. Nagashima, A.; Nuka, K.; Itoh, H.; Ichinokawa, T.; Oshima, C.; Otani, S. Surf Sci 1993, 291, 93.
14. Novoselov, K. S.; Geim, A. K.; Morozov, S. V.; Jiang, D.; Zhang, Y.; Dubonos, S. V.; Grigorieva, I. V.; Firsov, A. A. Science 2004, 306, 666.
15. Eda, G.; Chhowalla, M.; Nano Lett 2009, 9, 814.
16. Eda, G.; Emrah, U. H.; Rupesinghe, N.; Amaratunga, G. A. J.; Chhowalla, M. Appl Phys Lett 2008, 93, 233502.
17. Hua, H. T.; Wang, X. B.; Wang, J. C.; Wan, L.; Liu, F. M.; Zheng, H.; Chen, R.; Xu, C. H. Chem Phys Lett 2010, 484, 247.
18. Stankovich, S.; Piner, R. D.; Nguyen, S. T.; Ruoff, R. S. Carbon 2006, 44, 3342.
19. Schniepp, H. C.; Li, J. L.; McAllister, M. J.; Sai, H.; Herrera-Alonso, M.; Adamson, D. H.; Prud'Homme, R. K.; Car, R.; Saville, D. A.; Aksay, I. A. J Phys Chem B 2006, 110, 8535.
20. Halpin, J. C.; Kardos, J. L. Polym Eng Sci 1976, 16, 344.
21. Liang, J. J.; Huang, Y.; Zhang, L.; Wang, Y.; Ma, Y. F.; Guo, T. Y.; Chen, Y. S. Adv Funct Mater 2009, 19, 2297.
22. Kim, H.; Macosko, C. W. Macromolecules 2008, 41, 3317.
23. Lape, N. K.; Nuxoll, E. E.; Cussler, E. L. J Membr Sci 2004, 236, 29.
24. Kim, H.; Miura, Y.; Macosko, C. W. Chem Mater 2010, 22, 3441.